Spectral Evolution of Dark Asteroid Surfaces Induced by Space Weathering over a Decade

Sunao Hasegawa, Francesca Demeo, Michaël Marsset, Josef Hanuš, Chrysa Avdellidou, Marco Delbo, Schelte Bus, Hidekazu Hanayama, Takashi Horiuchi, Driss Takir, et al.

The Astrophysical Journal Letters, 939:L9 (12pp), 2022 November 1 https://doi.org/10.3847/2041-8213/ac92e4

Spectral Evolution of Dark Asteroid Surfaces Induced by Space Weathering over a Decade

Sunao Hasegawa[1], Francesca E. DeMeo[2], Michaël Marsset[2,3], Josef Hanuš[4], Chrysa Avdellidou[5], Marco Delbo[5], Schelte J. Bus[6], Hidekazu Hanayama[7], Takashi Horiuchi[8], Driss Takir[9], Emmanuël Jehin[10], Marin Ferrais[11], Jooyeon Geem[12,13], Myungshin Im[12,13], Jinguk Seo[12,13], Yoonsoo P. Bach[12,13], Sunho Jin[12,13], Masateru Ishiguro[12,13], Daisuke Kuroda[14], Richard P. Binzel[2], Akiko M. Nakamura[15], Bin Yang[16], and Pierre Vernazza[11]
[1] Institute of Space and Astronautical Science, Japan Aerospace Exploration Agency, 3-1-1 Yoshinodai, Chuo-ku, Sagamihara, Kanagawa 252-5210, Japan
hasehase@isas.jaxa.jp
[2] Department of Earth, Atmospheric and Planetary Sciences, MIT, 77 Massachusetts Avenue, Cambridge, MA 02139, USA
[3] European Southern Observatory (ESO), Alonso de Córdova 3107, 1900 Casilla Vitacura, Santiago, Chile
[4] Charles University, Faculty of Mathematics and Physics, Institute of Astronomy, V Holešovičkách 2, CZ-18000, Prague 8, Czech Republic
[5] Université Côte d'Azur, CNRS–Lagrange, Observatoire de la Côte d'Azur, CS 34229—F-06304 NICE Cedex 4, France
[6] Institute for Astronomy, University of Hawaii, 2860 Woodlawn Drive, Honolulu, HI 96822-1839, USA
[7] Ishigakijima Astronomical Observatory, National Astronomical Observatory of Japan, 1024-1 Arakawa, Ishigaki, Okinawa 907-0024, Japan
[8] Institute of Astronomy, University of Tokyo, 2-21-1 Osawa, Mitaka, Tokyo 181-0015, Japan
[9] Jacobs, NASA Johnson Space Center, Houston, TX 77058, USA
[10] Space Sciences, Technologies and Astrophysics Research Institute, Université de Liege, allée du 6 Août 17, B-4000 Liège, Belgium
[11] Aix Marseille Université, CNRS, CNES, Laboratoire d'Astrophysique de Marseille, Marseille, France
[12] Department of Physics and Astronomy, Seoul National University, Gwanak-gu, Seoul 08826, Republic of Korea
[13] SNU Astronomy Research Center, Seoul National University, Gwanak-gu, Seoul 08826, Republic of Korea
[14] Japan Spaceguard Association, Bisei Spaceguard Center, 1716-3 Okura, Bisei, Ibara, Okayama 714-1411, Japan
[15] Department of Planetology, Graduate School of Science, Kobe University, 1-1 Rokkodai-cho, Nada-ku, Kobe 657-8501, Japan
[16] Núcleo de Astronomía, Facultad de Ingeniería y Ciencias, Universidad Diego Portales, Av. Ejercito 441, Santiago, Chile
Received 2022 July 19; revised 2022 September 5; accepted 2022 September 16; published 2022 October 27

Abstract

The surfaces of airless bodies like asteroids in the solar system are known to be affected by space weathering. Experiments simulating space weathering are essential for studying the effects of this process on meteorite samples, but the problem is that the time spent to reproduce space weathering in these experiments is billions of times shorter than the actual phenomenon. In 2010 December, the T-type asteroid 596 Scheila underwent a collision with an impactor a few tens of meters in size. A decade later, there is an opportunity to study how the surface layer of this asteroid is being altered by space weathering after the impact. To do so, we performed visible spectrophotometric and near-infrared spectroscopic observations of 596 Scheila. The acquired spectrum is consistent with those observed shortly after the 2010 impact event within the observational uncertainty range. This indicates that the surface color of dark asteroids is not noticeably changed by space weathering over a 10 yr period. This study is the first to investigate color changes due to space weathering on an actual asteroid surface in the solar system. Considering that fresh layers are regularly created on asteroid surfaces by collisions, we suggest a genetic link between D/T-type and dark (low albedo) X-complex asteroids and very red objects such as 269 Justitia, 732 Tjilaki, and 203 Pompeja. New observations show that 203 Pompeja has an X-type-like surface, with some local surface areas exhibiting a very red spectrum.

Unified Astronomy Thesaurus concepts: Small solar system bodies (1469); Asteroids (72); Main belt asteroids (2036); Asteroid surfaces (2209)

1. Introduction

It is known that the surface layers of airless bodies in the solar system are usually not fresh, having been exposed to space for long periods of time. The effect responsible for altering the surfaces of these objects and affecting their colors and reflectance spectra is called space weathering. This process was first evidenced by the distinct colors of the youngest craters on the Moon (Gold 1955). Analysis of lunar soil samples then revealed that space weathering on the lunar surface is caused by the impact of micrometeoroids and implantation of solar wind (Hapke et al. 1975).

The lack of main belt asteroids with spectra similar to those of ordinary chondrites suggested that space weathering also affected the surface layers of S-complex asteroids (e.g., Pieters & McFadden 1994). Telescopic observations of S-complex and Q-type asteroids (Binzel et al. 1996) and rendezvous observations of S-complex asteroids by spacecraft (e.g., Veverka et al. 2000; Hiroi et al. 2006) later confirmed that space weathering causes changes in the reflectance spectra of the surfaces of S-complex asteroids. In particular, the samples returned from the S-complex asteroid 25143 Itokawa were compositionally similar to ordinary chondrites (e.g., Nakamura et al. 2011; Yurimoto et al. 2011). Nanophase iron particles, which had been found on the lunar soil (Keller & McKay 1993), were also found in the Itokawa samples (Noguchi et al. 2011), thereby proving that the reflectance spectra of S-complex asteroids are reddened by space weathering.

For a long time, space weathering of dark asteroids (albedo values less than 0.1), such as C-complex and D-type asteroids, did not receive much attention because many dark asteroids had been found to exhibit spectra consistent with carbonaceous chondrites (e.g., Clark et al. 2002). Nesvorný et al. (2005) was

the first to show a trend in space weathering of C-complex asteroids based on correlations between family ages and spectral slopes. Lantz et al. (2018) further showed trends in spectral slope due to space weathering for each spectral type of dark asteroids observed from telescopic and laboratory study data.

Laboratory simulation experiments of space weathering using minerals and meteorites are very important for understanding spectral changes in response to this process on the surface of asteroids (e.g., Moroz et al. 1996; Dukes et al. 1999; Yamada et al. 1999). In particular, the results of simulated space weathering experiments on carbonaceous chondrites, which are considered to be the meteorite counterparts of dark asteroids, are essential to understand the spectral changes induced by space weathering on this type of object (e.g., Vernazza et al. 2013; Matsuoka et al. 2015; Lantz et al. 2017). While laboratory experiments are important research methods for understanding space weathering, there is one obstacle that cannot be overcome: time-simulated experiments alter the spectra of the exposed samples over milliyear timescales, whereas the spectral changes induced by space weathering on actual asteroids act over thousand-year timescales or more. Although the irradiating fluxes are increased billions of times in intensity with respect to actual space weathering during the experiments, it cannot be guaranteed that this properly reproduces what is happening in nature over such long timescales. If experiments could be performed on meteorites such that they match the space-weathered age of the actual observed asteroid, and if the resulting irradiated meteorite and the asteroid spectra could be compared, this problem would be resolved.

Another point of interest is the characteristic time over which space weathering significantly affects the spectra. Studies combining asteroid spectra with the age of their respective collisional families showed spectral changes in response to space weathering over million- to billion-year timescales (Nesvorný et al. 2005; Vernazza et al. 2009). In addition, space weathering has been reported to be efficient over thousand-year timescales, although this was reported for ordinary chondrites instead of carbonaceous chondrites (Jin & Ishiguro 2022; Noguchi et al. 2014). However, it remains unknown how spectra change due to space weathering over shorter time periods. In particular, it would be very interesting to know if the spectral slope changes linearly or logarithmically with time over periods shorter than a thousand to a million years.

The surface of the T-type asteroid 596 Scheila, with an albedo of 0.038,[17] was refreshed during an impact with a projectile a few tens of meters in size in 2010 (Ishiguro et al. 2011a, 2011b). In this collision event, the spectral type of 596 turned redder, from T type to D type (Hasegawa et al. 2022). Assuming that the surface layer of 596 was space weathered before the impact, and that a fresh surface appeared after the event, it was concluded that objects compositionally similar to 596 become bluer in spectral slope due to space weathering. This year marks approximately 10 yr since the collisional event. This means that the refreshed surface of 596 has been exposed to space weathering for a period of approximately 10 yr. To test whether the surface layer of 596 and its reflectance spectrum changed during that period of time, we performed spectral observations of 596 in 2022, more than a decade after the collisional event.

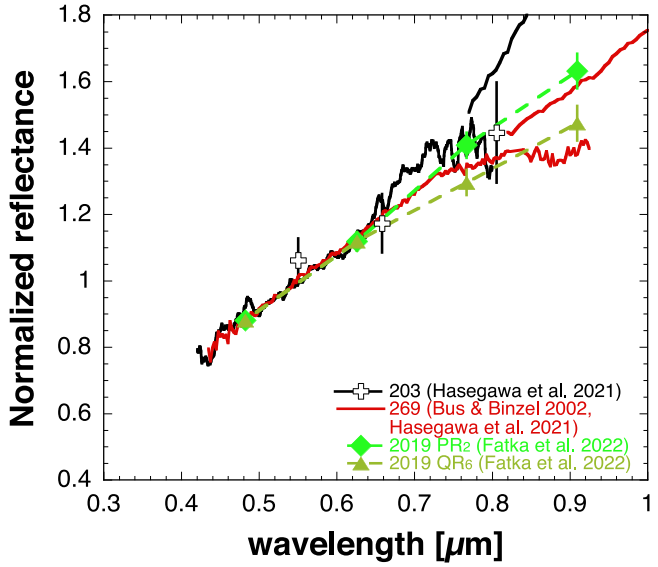

Figure 1. Comparison of the visible spectra of VROs 203 Pompeja, 269 Justitia, 2019 PR_2, and 2019 QR_6. The figure shows the spectra in the 0.4–1.0 μm wavelength regions, normalized to 1 at 0.55 μm.

In this study, we investigate the spectral changes caused by space weathering over a short timescale of 10 yr, which is a much shorter timescale than the formation age of the solar system. A comparable study of asteroids over a short timescale of 300 yr was recently reported by Fatka et al. (2022). These authors found that two near-Earth asteroids (NEAs), 2019 PR_2 and 2019 QR_6, may have formed as a pair about 300 yr ago. The authors also showed that the two asteroids have spectral slopes that are equal to or redder than those of D-type asteroids. This suggests that the fresh surface layers of D-type asteroids before space weathering effects become apparent may be similar to the very red objects (VROs) found by Hasegawa et al. (2021), which have a redder spectral slope than the average D-type asteroid (DeMeo et al. 2009; Hasegawa et al. 2022). Figure 1 shows that the very red NEAs, which may be very young, have a similar slope in visible spectra to the VROs 203 Pompeja, with an albedo of 0.045 (see footnote 17), and 269 Justitia, with an albedo of 0.080 (see footnote 17). This indicates that the surface ages of 203 and 269 may be as young as a few hundred years. Therefore, we also conducted observations of 203 and 269 to investigate if a slope change occurred in their spectra over time. Note that one further VRO, 732 Tjilaki, with an albedo of 0.068,[18] was discovered by Bourdelle de Micas et al. (2022). We also investigated if a slope change occurred in the 732 spectra over time using literature.

2. Observations and Data Analysis

New near-infrared (NIR) observations of 596 Scheila were carried out with the SpeX NIR spectrograph (Rayner et al. 2003) on the 3.2 m NASA Infrared Telescope Facility (IRTF) located on Maunakea, Hawaii, on 2022 April 4. Both Landolt 102-1081 and Landolt 107-998 were used as solar analogs for the NIR observation (Marsset et al. 2020). Reduction of NIR

[17] Mean values obtained from IRAS (Tedesco et al. 2002), AKARI (Usui et al. 2011), and WISE (Masiero et al. 2011).

[18] Mean values obtained from IRAS (Tedesco et al. 2002) and AKARI (Usui et al. 2011).

spectral images was conducted using IRAF (Tody 1993) and IDL. Close in time, visible observations were conducted in the synchronous imaging camera with the g', R_C, and I_C bands (Yanagisawa et al. 2010) on the 1.05 m Murikabushi Telescope located on Ishigakijima, Japan, on 2022 February 8. Object HD 142801 was used as a calibration star for the visible observation. Data reduction for photometry was performed using IRAF. The procedures for the NIR and visible observations and reduction are as described in Binzel et al. (2019) and Hasegawa et al. (2021), respectively.

The NIR spectrum of 269 Justitia was collected on 2009 June 15 using SpeX/IRTF (J. P. Emery 2022, private communication). Object HD 124901 was used as a solar analog star. Spectral images were reduced by IDL. The procedures for the NIR observations and reduction of 269 are as described in Emery et al. (2011).

The NIR spectra of 203 Pompeja were obtained on 2020 December 1 and 2022 June 10 and 27. As in previous observations, the observations were made using SpeX/IRTF. BD+00 2717, HD 249566, and HD 106116 were used as solar analog stars on 2020 December 1, 2022 June 10, and 2022 June 27, respectively. Reduction of the spectroscopic images was performed with IDL. The procedures for the NIR observations and reduction of 203 are as described in Takir & Emery (2012) and Avdellidou et al. (2021). Visible spectra of 203 Pompeja were obtained on 2022 June 18, 19, 29, and 30. Colorimetric observations were acquired with the robotic telescope TRAPPIST-South (TS; Jehin et al. 2011), located at the ESO La Silla Observatory in Chile. It is a 0.6 m Ritchey–Chrétien telescope operating at $f/8$ and equipped with a thermoelectrically cooled FLI ProLine 3041-BB CCD camera. The data were reduced using PHOTOMETRYPIPELINE (Mommert 2017) and calibrated to the band in which they were observed using the Pan-STARRS catalog.

3. 596 Scheila

3.1. Spectroscopic Results

We compared the spectra of 596 Scheila obtained before, immediately after, and a decade after the 2010 impact to search for any spectral change induced by space weathering. Spectral data before the 2010 impact event are from Bus & Binzel (2002) and DeMeo et al. (2009). The NIR spectral data obtained immediately after the impact event were retrieved from Yang & Hsieh (2011) and Hasegawa et al. (2022). Visible spectrophotometric data from immediately after impact were combined from Trigo-Rodriguez et al. (2011), Betzler et al. (2012), Hsieh et al. (2012), Jewitt (2012), and Shevchenko et al. (2016). In addition to the data acquired in the present work, multifilter photometric data from Sergeyev et al. (2022) were used as part of the "10 yr after the event" data set, as those data were obtained on 2018 August 20. As reference data, the visible reflectance spectrum from Gaia, which is an average of several observations taken somewhere between 2014 August 5 and 2017 May 28, i.e., ∼3.5 and ∼6.5 yr after the impact event is also shown (Gaia Collaboration et al. 2022).[19] Table 1 indicates the subobserver coordinates of NIR observations before, immediately after, and a decade after the impact, calculated based on the shape model of 596 from Hanuš et al. (2021). Although the observed latitude and longitude of each observation are different, Hasegawa et al. (2022) indicated that the ejecta discharged by the 2010 impact event was deposited over the entire surface of the asteroid and that the surface layer was homogeneously covered by fresh material.

Figure 2 compares the reflectance spectra of 596 before, immediately after, and 10 yr after the impact event. The spectral slope of 596 over 0.8–2.5 μm before, immediately after, and a decade after the impact event is 25.5%, 46.7% (40.5%), and 42.2% μm^{-1}, respectively. The slopes of the NIR spectra immediately after the impact and about 10 yr after the impact are consistent within the expected slope uncertainty of 4.2% μm^{-1} for SpeX measurements (Marsset et al. 2020). The slope consistency between the visible spectra of 596 obtained over all observed periods indicates no significant change over the decade at these wavelengths within the observational uncertainty range.

3.2. Spectral Changes Due to Phase Angle

Regarding possible changes in the spectral gradient, it was shown in Hasegawa et al. (2022) that the particle size effect cannot explain the observed spectral reddening changes. However, the possibility of a change in the slope of the spectrum due to a change in roughness and phase angle was not discussed in Hasegawa et al. (2022) and is discussed below.

Binzel et al. (2015) pointed out that spectral changes occur due to surface roughness effects in the case of regolith-free surfaces. However, the surface layer of 596 is considered to be covered with regolith (Ishiguro et al. 2011a; Yang & Hsieh 2011). Therefore, changes in spectral slope due to roughness do not need to be taken into account in the case of 596.

Sanchez et al. (2012) described the spectral dependence on the phase angle of ordinary chondrites. For ordinary chondrites, changes in spectral slope are not detected below a phase angle of 30° (Figure 3). Considering that our measurements of the spectral slope were obtained in the range of phase angle values comprised between 0.4° and 19.2° degrees, we do not expect them to be significantly affected by a change in phase angle. Thomas et al. (2014) investigated the spectral dependence on the phase angle of S-type asteroids 433 Eros, 1036 Ganymed, and 1627 Ivar. Among these objects, 433 Eros was shown to be spectrally homogeneous across its surface by NASA's spacecraft NEAR Shoemaker (Bell et al. 2002). No significant change in the spectral slope of 433 can be observed up to a phase angle of ∼22° (Figure 3). This, again, argues against phase angle as being responsible for a change in spectral slope in our observations considering the small range of phase angles in our observations.

While there are examples of phase angle dependence for S-type asteroids as described above, no studies have investigated the phase angle dependency of the spectral slope of individual D-type asteroids. However, there are examples where spectra of various D-type asteroids have been collected to investigate the dependence of the spectral slope on the phase angle in the visible-to-NIR wavelength range (Lantz et al. 2018). The D-type asteroids have been shown to have an increasing spectral slope with increasing phase angle, but, given the uncertainty in the slope of the observations presented in Marsset et al. (2020), it is not possible to state the change in the slope of the spectrum within a phase angle between ∼2° and ∼19° considering the number of available measurements (Figure 3). However, this data set used data from different

[19] The epoch spectra are not available in the Data Release 3 (DR3). All of the DR3 asteroid spectra are averages of epoch spectra taken between 2014 August 5 and 2017 May 28.

Table 1
Subobserver Coordinates of 596 Scheila during NIR Observations Based on Hanuš et al. (2021)

Observation Time	Timing of Observation	Sub-Earth point				Spectral Slope (% μm^{-1})	R_h[c] (au)	Δ[c] (au)	α[c] (deg)	Reference
		λ_1[a] (deg)	ϕ_1[a] (deg)	λ_2[b] (deg)	ϕ_2[b] (deg)					
2002/06/01 09:40	Before impact	137	46	232	−47	25.5	2.45	1.43	0.4	DeMeo et al. (2009)
2011/01/04 14:50	Immediately after impact	132	−39	263	43	40.5[d]	3.07	2.26	12.0	Yang & Hsieh (2011)
2011/01/05 14:20	Immediately after impact	319	−39	90	44	40.5[d]	3.07	2.25	11.7	Yang & Hsieh (2011)
2011/02/07 09:31	Immediately after impact	99	−40	225	50	46.7	3.02	2.07	6.4	Hasegawa et al. (2022)
2022/04/09 14:29	A decade after impact	357	51	179	−42	42.2	2.46	1.73	19.2	This work

Notes.
[a] Pole solution 1: $\lambda_1 = 110$ (deg), $\beta_1 = -24$ (deg), period = 15.8605 (hr).
[b] Pole solution 2: $\lambda_2 = 273$ (deg), $\beta_2 = -38$ (deg), period = 15.8609 (hr).
[c] The heliocentric (R_h) and geocentric distances (Δ) and phase angle (α) for asteroid observations were taken from the NASA/Jet Propulsion Laboratory HORIZONS ephemeris generator system. https://ssd.jpl.nasa.gov/horizons.
[d] The value of the combined spectrum in Yang & Hsieh (2011).

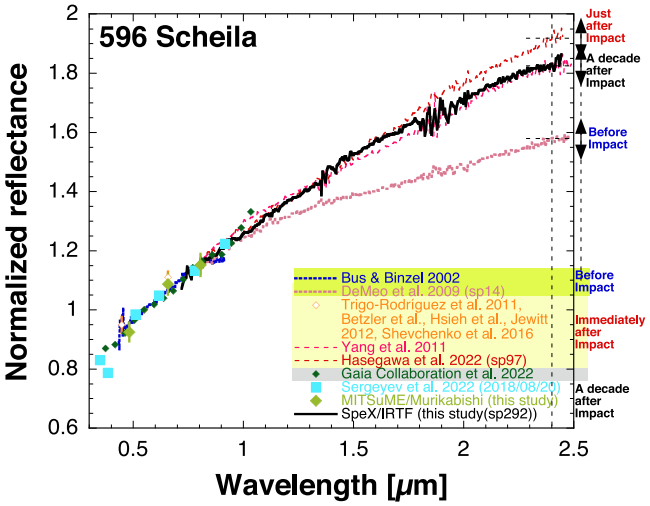

Figure 2. Comparison of 596 Scheila's NIR spectra before, immediately after, and a decade after the 2010 impact event. The figure shows spectra of 596 in the 0.4–2.5 μm wavelength region, normalized to 1 at 0.55 μm. The black arrows indicate the slope uncertainty from Marsset et al. (2020) centered at the reflectance value of the spectra at 2.40 μm, as shown by the black dashed lines.

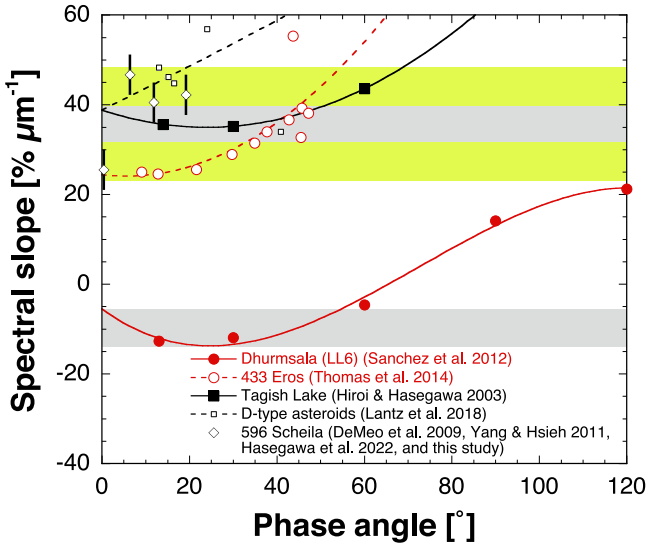

Figure 3. Comparison between the spectral slopes of the Dhurmsala (LL6) and Tagish Lake (C2) meteorites, Sw-type asteroid 433 Eros, and D-type asteroids as a function of phase angle. The D-type asteroid data set is a combination of multiple D-type asteroids. Gray and yellow areas indicate the slope uncertainty from Marsset et al. (2020) for the meteorites and asteroids, respectively. The solid and dashed lines represent polynomial fits for the meteorites and asteroids, respectively. The D-type data set includes the postimpact spectrum of 596.

D-type asteroids, which may have different spectral slopes at a given phase angle. Hiroi & Hasegawa (2003) studied the spectral slope of the Tagish Lake meteorite by varying the phase angle. The slope of the spectrum does not change up to a phase angle of 30°, but the slope of the spectrum increases slightly at a phase angle of 60° (Figure 3). However, up to within ∼50° of the phase angle, the change is within the range of observation uncertainty. Therefore, with 596 having a spectrum comparable to that of the Tagish Lake meteorite, one cannot expect to detect a slope change at phase angles below ∼50°.

The NIR observations of 596 before and after the 2010 impact cover a range of phase angles between 0°.4 and 19°.2. Considering that the spectral slope of 596 varies beyond about three times the observation uncertainty, it can be concluded that the spectral changes are not due to changes caused by the phase angle.

3.3. Constraints on Spectral Changes Due to Space Weathering

The spectral match between the spectrum of the fresh surface observed immediately after the 2010 impact event and the space-weathered one observed a decade later indicates that the spectra of dark asteroids like 596 do not evolve over a decade timescale due to space weathering. This was predicted from a number of space weathering experiments performed on carbonaceous chondrites (e.g., Vernazza et al. 2013; Matsuoka et al. 2015; Lantz et al. 2017). However, this is the first time that the absence of spectral changes due to space weathering is observationally confirmed for an actual asteroid under conditions where the exposure time is precisely known.

Next, we investigate whether the spectral change due to space weathering acts linearly or logarithmically with time. Following Ishiguro et al. (2011b), we assume that the impact on 596 occurred on 2010 December 3. Then, considering that the average collisional lifetime of 596 for impacts of the scale of the 2010 event is about 10^4 yr (Hasegawa et al. 2022), we assume that this was the age of 596's surface just before the impact, when the spectrum of DeMeo et al. (2009) was acquired. Under these assumptions, we fit both a linear and a logarithmic function to the slope values of the spectra from Yang & Hsieh (2011; $t = 0.09$ yr after the collision), Hasegawa et al. (2022; $t = 0.18$ yr), and DeMeo et al. (2009; $t = 10^4$ yr). By doing so, we find that the slope would have changed by $0.0018\%\ \mu m^{-1}\ yr^{-1}$ assuming a linear evolution and $3.6\%\ \mu m^{-1}\ (\log(yr))^{-1}$ assuming a logarithmic evolution (Figure 4). That is, if space weathering changes linearly, the expected slope after about 10 yr would be $43.6\%\ \mu m^{-1}$, while if it changes logarithmically, the expected slope after about 10 yr would be $36.4\%\ \mu m^{-1}$. The actual slope we observed after about 10 yr is 42.2%, meaning that the change is smaller than the expected value from the logarithmic function, although 1.5σ is consistent considering the expected $4.2\%\ \mu m^{-1}$ measurement uncertainty (Marsset et al. 2020). This suggests that the spectral change slope evolution due to space weathering during the first decade is not logarithmic with respect to time, but linear. Therefore, we find that the NIR reflectance spectra of reddish dark asteroids like 596 likely do not evolve faster than a logarithmic function, at least during the first 10 yr following a refreshing event.

4. 269 Justitia

The visible spectra of 269 Justitia measured on 1994 November 5 and 2010 January 11 were retrieved from Bus & Binzel (2002) and Cellino et al. (2020), respectively. Most data collected on 2018 July 16 were retrieved from Sergeyev et al. (2022). The mean visible spectra were also obtained somewhere between 2014 August 5 and 2017 May 28 (Gaia Collaboration et al. 2022; see footnote 19). These visible spectra of 269 at 0.45–0.85 μm are consistent with one another (Figure 5). This indicates that the visible spectrum of 269 at 0.45–0.85 μm did not change over 22 yr. Two NIR spectra of 269 were acquired on 2002 September 28 (Hasegawa et al. 2021) and 2005 May 11 (DeMeo et al. 2009). Moreover, the

Table 2
Subsolar and Observer Coordinates of 203 Pompeja during Photometric and Spectral Observations

Observation Time	Telescope	Subsolar Point				Sub-Earth Point				Reference
		λ_1[a] (deg)	ϕ_1[a] (deg)	λ_2[b] (deg)	ϕ_2[b] (deg)	λ_1[a] (deg)	ϕ_1[a] (deg)	λ_2[b] (deg)	ϕ_2[b] (deg)	
1988/10/06 08:15	McDonald	60	−1	234	2	51	11	225	−10	Sawyer (1991)
2018/04/16 14:37–54	SkyMapper	21–16	−4	202–197	4	15–10	−13	194–190	11	Sergeyev et al. (2022)
2018/04/17 13:55	SkyMapper	32	−4	212	4	26	−13	205	11	Sergeyev et al. (2022)
2018/04/21 14:14–30	SkyMapper	30–26	−5	211–207	4	25-21	−13	204–200	311	Sergeyev et al. (2022)
2018/04/22 13:42	SkyMapper	39	−5	219	5	34	−13	213	11	Sergeyev et al. (2022)
2018/05/15 14:11–12	SkyMapper	47	−9	228	8	49	−9	228–227	7	Sergeyev et al. (2022)
2019/09/01 13:36	SkyMapper	334	−48	156	49	340	−50	162	50	Sergeyev et al. (2022)
2019/09/07 09:48	SkyMapper	34	−48	216	48	44	−50	226	50	Sergeyev et al. (2022)
2020/12/01 08:21	IRTF	332	29	153	−28	337	35	156	−32	This work
2021/01/14 09:08	IRTF	357	36	179	−36	9	29	189	−26	Hasegawa et al. (2021)
2021/01/29 12:55	SAO(Spec)	310	39	132	−38	326	28	146	−26	Hasegawa et al. (2021)
2021/02/04 10:36	SAO(Phot)	348	39	170	−39	5	27	189	−26	Hasegawa et al. (2021)
2022/06/10 05:41	IRTF	341	17	163	−17	357	31	175	−33	This work
2022/06/18 23:27	TRAPPIST	80	16	262	−16	97	30	277	−32	This work (BVR_CI_C)
2022/06/19 01:02	TRAPPIST	57	16	239	−16	73	30	253	−32	This work (BVR_CI_C)
2022/06/19 02:43	TRAPPIST	32	16	213	−16	48	30	228	−32	This work (BVR_CI_C)
2022/06/27 08:08	IRTF	316	14	138	−15	332	29	152	−31	This work
2022/06/29 00:18	TRAPPIST	75	14	257	−15	91	29	271	−31	This work (BVR_CI_Cz')
2022/06/29 23:15	TRAPPIST	91	14	273	−14	107	28	287	−31	This work (BVR_CI_Cz')
2022/06/30 00:57	TRAPPIST	66	14	248	−14	82	28	262	−30	This work (BVR_CI_Cz')
2022/06/30 02:30	TRAPPIST	43	14	225	−14	58	28	239	−30	This work (BVR_CI_C)

Notes.
[a] Pole solution 1: $\lambda_1 = 315$ (deg), $\beta_1 = -40$ (deg), period = 24.0550 (hr).
[b] Pole solution 2: $\lambda_2 = 132$ (deg), $\beta_2 = -36$ (deg), period = 24.0551 (hr).

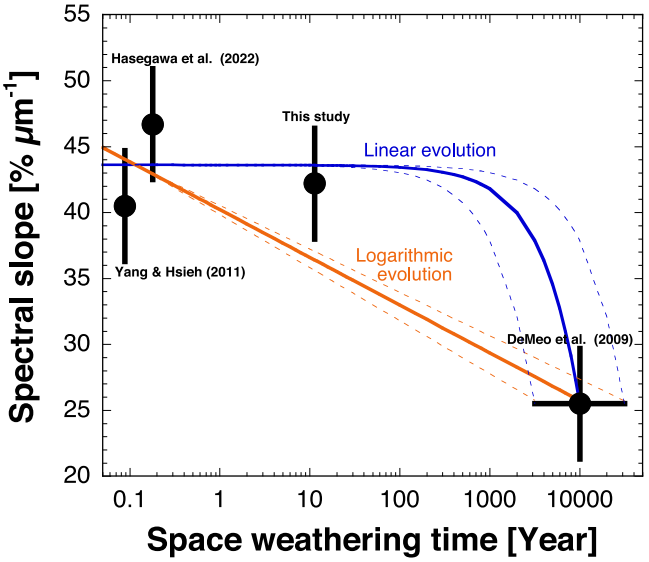

Figure 4. Spectral slope for 596 Scheila against space weathering time. Blue and orange lines correspond to linear and logarithmic regression of the spectral slope values of DeMeo et al. (2009), Yang & Hsieh (2011), and Hasegawa et al. (2022), respectively.

NIR spectrum of 269 was obtained on 2009 June 15 (J. P. Emery, private communication). The slopes of the three NIR data between 0.8 and 0.95 μm are consistent with the slope of the visible data from Sergeyev et al. (2022; Figure 5).

The slope of the visible spectrum of 269 between 0.45 and 0.95 μm is found to have remained unchanged for at least about 16 yr. Although the observed wavelengths are different, the results of the unchanged spectra are the same for 269 and 596.

5. 732 Tjilaki

Visible spectra of 732 Tjilaki were obtained on 1992 March 4 (Xu et al. 1995), 1997 March 7 (Lazzaro et al. 2004), and 2021 October 1 (Bourdelle de Micas et al. 2022). The mean visible spectra were also acquire between 2014 August 5 and 2017 May 28 (Gaia Collaboration et al. 2022; see footnote 19). The NIR spectra were obtained on 2021 October 23 (Bourdelle de Micas et al. 2022). These visible spectra of 732 at 0.6–0.9 μm are consistent with one another (Figure 5).

The slope of the visible spectrum of 732 between 0.6 and 0.9 μm has not changed for at least about 29 yr. We conclude that the spectra of 732 have not changed within the observed time interval, which is consistent with our results for 269 or 596.

6. 203 Pompeja

For 203 Pompeja, a visible spectrum, visible spectrophotometric color, and NIR spectrum were taken on 2021 January 29, February 4, and January 14, respectively (Hasegawa et al. 2021). Meanwhile, most of the data from Sergeyev et al. (2022) for 203 were acquired from 2018 April 16 to May 15. The visible spectra of 203, which were acquired by Sawyer (1991) and Gaia Collaboration et al. (2022; see footnote 19), match the one of Sergeyev et al. (2022). The slope of the spectrum of 203 obtained by Hasegawa et al. (2021) is redder than that of a typical D type, but the slope of the spectrum obtained by Sergeyev et al. (2022) is comparable to that of a T type (Figure 5). In addition, new visible and NIR spectra of 203 were obtained on 2022 June 18, 19, 29, and 30; 2020 December 1; and 2022 June 10 and 27 and classified as X types. The above indicates that there is a large slope variation of the visible and NIR spectra of 203 acquired in Hasegawa et al. (2021) with respect to the other years. Moreover, the latitude and longitude of the sub-Earth point at the time of both observations by IRTF coincide (see Table 2). Table 2 was based on the shape model of 203 from Appendix A.

The fact that the NIR spectra of other asteroids obtained using the same solar analog stars on the same date as Hasegawa et al. (2021) are consistent with previous spectra gives credit to this NIR spectrum of 203 (see Appendix B). Additional visible data for three other asteroids obtained by the same surveys as 203 are highly consistent with the data from Sergeyev et al. (2022) and Gaia Collaboration et al. (2022; see Appendix C). Therefore, it appears that the visible spectrum and spectrophotometric color reported in Hasegawa et al. (2021) are valid. Furthermore, the slope of the measured visible spectrum (0.7–0.8 μm) is consistent with the slope in the NIR spectrum (0.8–0.9 μm), which further validates the observational result of Hasegawa et al. (2021).

The first possible cause of the spectral differences is cometary activity, as reported on 596. Therefore, the radial profiles of 203 around the observation period of Hasegawa et al. (2021) were investigated by comparing the radial profiles with field stars to detect a faint comet-like coma. However, no coma is detected within the background detection limit of 25.1 mag arcsec^{-2} in the r band (see Appendix D). This evidence suggests that the spectral differences may not be triggered by unforeseen cometary activity.

The only difference between the IRTF observations is the latitude of the subsolar point. The subsolar points were at relatively high latitudes[20] in the 2021 observations (Table 2). The existence of regions with a VRO-like spectrum in high latitudes is necessary to explain the spectral differences. There may be a giant crater that is shaded under a low subsolar point and whose areas are not visible, such as the giant crater on asteroid 253 Mathilde (Veverka et al. 1997). Since the VRO-like spectra are much brighter in the NIR than the X-type spectra, even if the area of the crater illuminated by sunlight is small, the feature may appear in the spectrum. An asteroid with surface heterogeneity was also reported in Avdellidou et al. (2021). These authors suggested that the very red spectrum may correspond to a fresh crater formed by an impact, as their studied asteroid, 223 Rosa, also showed a very red spectrum when observed at different epochs. Finding craters with a VRO-like color on asteroids with an X-type surface implies that asteroids with a VRO surface layer evolved to an X-type-like surface layer by space weathering. If solar wind is the main cause of space weathering, the time of sunlight exposure at the bottom of craters such as this one, where sunlight is less directly illuminated, is much shorter than on other surfaces, so that the time for sunlight penetration is relatively longer and the spectral features may not disappear. Considering that VROs have the same spectral properties as RR- and IR-class trans-Neptunian objects (Fulchignoni et al. 2008; Fraser et al. 2022), this supports the proposal of Vernazza et al. (2021) and Rivkin et al. (2022) that D/T-type and dark X-complex asteroids originated from the same transplanetary and/or trans-Neptunian planetesimal region.

[20] This is applied to the first shape/pole model, whereas the second shape/pole solution has the northern and southern hemispheres reversed.

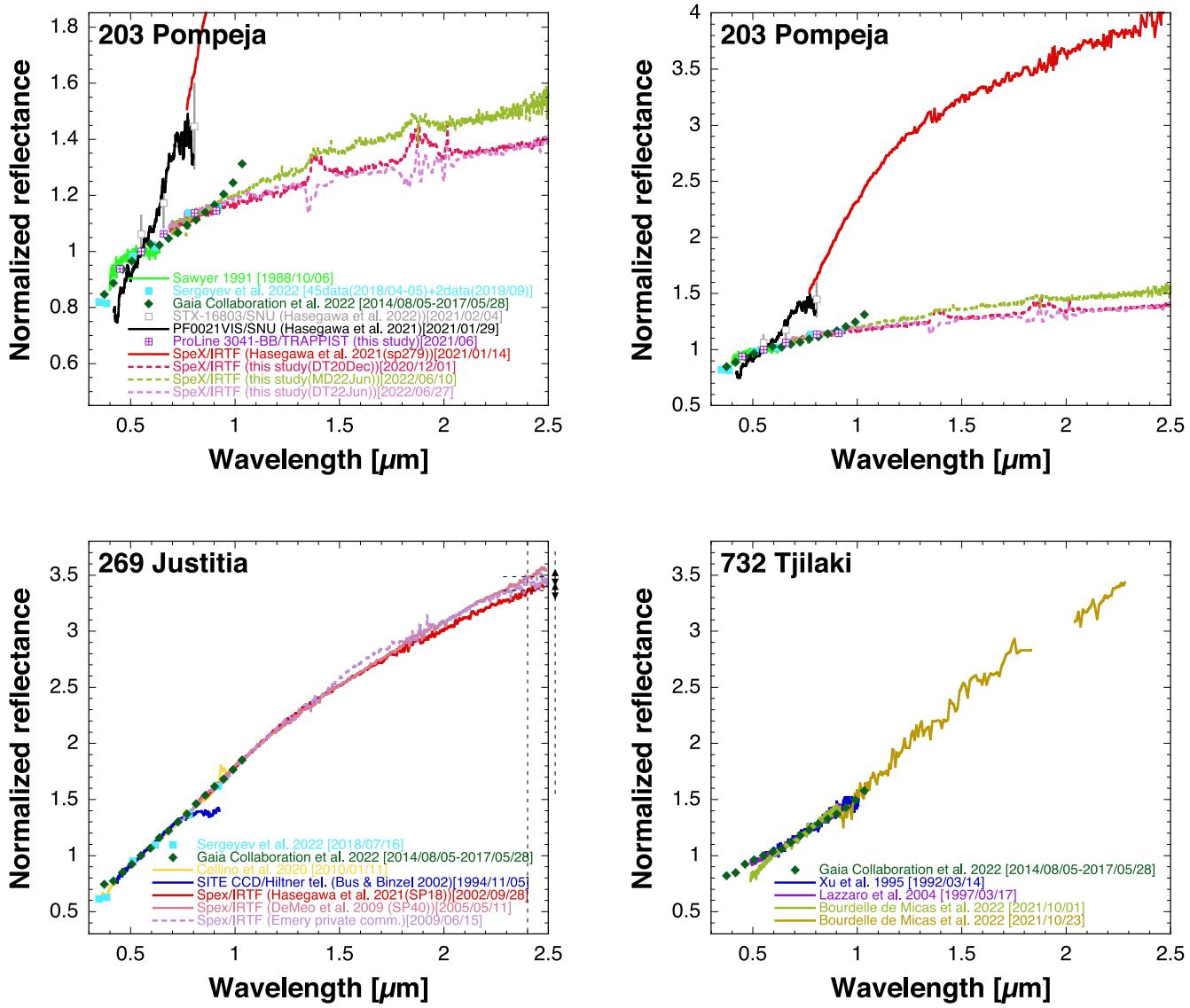

Figure 5. Spectra of 203 Pompeja (top panels), 269 Justitia (bottom left panel), and 732 Tjilaki (bottom right panel). Square brackets in these panels indicate the observation dates. Black arrows are present on the right-hand side of the vertical axis in the 269 figure. Arrows indicate the slope uncertainty from Marsset et al. (2020) centered at the reflectance value of the spectra at 2.40 μm, as shown by the black dashed lines.

7. Conclusions

A comparative study of the spectra of the T/D-type asteroid 596 Scheila before, immediately after, and 10 yr after the 2010 impact event reveals the following.

1. Fresh surfaces on dark asteroids with reddish spectra like 596 do not undergo any noticeable spectral changes induced by space weathering over a 10 yr timescale.
2. This is the first time that the absence of spectral changes due to space weathering has been measured over an accurate time interval for an actual asteroid, as opposed to meteorite samples measured in laboratory simulations.
3. During the first decade of space weathering following a resurfacing event, the spectral change progression of dark and reddish asteroids does not appear to progress logarithmically, but linearly.

Applying the findings of our study to VROs 203 Pompeja, 269 Justitia, and 732 Tjilaki, we can suggest the following.

1. The spectrum of 203 Pompeja was found to be a VRO in the 2021 observations but an X type in the other observational epoch. The existence of a giant crater with a VRO spectrum in one of the polar regions is suggested to explain this spectral difference. This would imply that the spectra of VROs evolve into dark X types as space weathering progresses over time.
2. Combining the results from the study of Fatka et al. (2022) on asteroid pairs and our own results, it is possible that the spectral slope of VROs remains mostly unchanged over a timescale of 300 yr.

We would like to thank the referee for the careful review and constructive suggestions, which helped us to improve the manuscript significantly. We are grateful to Dr. Joshua P. Emery for sharing valuable 269 data and supporting 203 observations. We greatly appreciate Dr. Petr Fatka and Dr. Nicholas A. Moskovitz for useful information about their observed NEAs. This work is based on observations collected

at the Infrared Telescope Facility, which is operated by the University of Hawaii under contract 80HQTR19D0030 with the National Aeronautics and Space Administration, Ishigaki-jima Astronomical Observatory, National Astronomical Observatory of Japan, and at Seoul National University Astronomical Observatory. The authors acknowledge the sacred nature of Maunakea and appreciate the opportunity to observe from the mountain. The instrumentation at IAO was supported by a Grant-in-Aid for Scientific Research on Priority Areas (19047003). TRAPPIST is a project funded by the Belgian Fonds (National) de la Recherche Scientique (F.R.S.-FNRS) under grant PDR T.0120.21. We thank the Las Cumbres Observatory and its staff for its continuing support of the ASAS-SN project. ASAS-SN is supported by the Gordon and Betty Moore Foundation through grant GBMF5490 to the Ohio State University and funded in part by Alfred P. Sloan Foundation grant G-2021-14192 and NSF grant AST-1908570. Development of ASAS-SN has been supported by NSF grant AST-0908816, the Mt. Cuba Astronomical Foundation, the Center for Cosmology and AstroParticle Physics at the Ohio State University, the Chinese Academy of Sciences South America Center for Astronomy (CAS-SACA), the Villum Foundation, and George Skestos. This work has made use of data from the Asteroid Terrestrial-impact Last Alert System (ATLAS) project. ATLAS is primarily funded to search for near-Earth asteroids through NASA grants NN12AR55G, 80NSSC18K0284, and 80NSSC18K1575; by-products of the NEO search include images and catalogs from the survey area. The ATLAS science products have been made possible through the contributions of the University of Hawaii Institute for Astronomy, the Queen's University Belfast, the Space Telescope Science Institute, the South African Astronomical Observatory (SAAO), and the Millennium Institute of Astrophysics (MAS), Chile. The ZTF data were based on observations obtained with the Samuel Oschin Telescope 48 inch and the 60 inch telescope at the Palomar Observatory as part of the Zwicky Transient Facility project. The ZTF is supported by the National Science Foundation under grant No. AST-2034437 and a collaboration including Caltech, IPAC, the Weizmann Institute for Science, the Oskar Klein Center at Stockholm University, the University of Maryland, Deutsches Elektronen-Synchrotron and Humboldt University, the TANGO Consortium of Taiwan, the University of Wisconsin at Milwaukee, Trinity College Dublin, Lawrence Livermore National Laboratories, and IN2P3, France. Operations are conducted by COO, IPAC, and UW. This study has utilized the SIMBAD database, operated at CDS, Strasbourg, France, and the JPL HORIZONS ephemeris generator system, operated at JPL, Pasadena, USA. This work is based on data provided by the Minor Planet Physical Properties Catalogue (MP3C) of the Observatoire de la Côte d'Azur. F.D. and M.M. were supported by the National Aeronautics and Space Administration under grant Nos. 80NSSC18K0849 and 80NSSC18K1004 issued through the Planetary Astronomy Program. Any opinions, findings, and conclusions or recommendations expressed in this letter are those of the authors and do not necessarily reflect the views of the National Aeronautics and Space Administration. The work of J.H. has been supported by the Czech Science Foundation through grant 20-08218S. C.A. and M.D. acknowledge support from ANR "ORIGINS" (ANR-18-CE31-0014). C.A. and M.D. were Visiting Astronomers at the Infrared Telescope Facility, which is operated by the University of Hawaii under contract 80HQTR19D0030 with the National Aeronautics and Space Administration. E.J. is FNRS Senior Research Associate. M.Im acknowledges the support from the Korea Astronomy and Space Science Institute grant under the R&D program (project No. 2020-1-600-05) supervised by the Ministry of Science and Technology and ICT (MSIT), and the National Research Foundation of Korea (NRF) grant, No. 2020R1A2C3011091, funded by MSIT. M.I. was supported by NRF grant No. 2018R1D1A1A09084105. This study was supported by JSPS KAKENHI (grant Nos. JP20K04055, JP21H01140, JP21H01148, and JP22H00179) and the Hypervelocity Impact Facility (former facility name: the Space Plasma Laboratory), ISAS, JAXA.

Facilities: IRTF:3.2 m, Murikabushi:1.05 m, SAO:1.0 m, TRAPPIST-South:0.6 m, ZTF:1.2 m.

Software: IRAF (Tody 1993), IDL.

Appendix A
Shape Model of 203 Pompeja

In order to link the measured spectra of 203 Pompeja to their corresponding regions on its surface (i.e., to derive the subobserver points), the knowledge of the rotation state (i.e., sidereal rotation period and orientation of the spin axis) is necessary. However, 203's shape model and rotation state have not been derived so far. To fix this, we compiled available optical data of 203 and applied the convex inversion. This light-curve inversion method developed by Kaasalainen & Torppa (2001) and Kaasalainen et al. (2001) was already successfully used for the 3D shape and rotation state determination of more than 3400 asteroids (see the Database of Asteroid Models from Inversion Techniques[21]; Durech et al. 2010). Therefore, convex inversion is a well-tested state-of-the art method for the shape modeling of asteroids. Here we follow the standard modeling approach described in detail in, for instance, Athanasopoulos et al. (2022) and Hanuš et al. (2021).

Our optical data set includes 18 dense light curves from two apparitions: in 1983 (Di Martino 1984) and 2011/2012 (Pilcher et al. 2012). In particular, the latter data set is highly valuable, as the authors dedicated a large effort in reliably deriving the rotation period of 203. The main difficulty stems from the rotation period being very close to 24 hr. The rotation phase cannot then be fully sampled from one location on the Earth; rather, multiple observers at different longitudes have to participate in the campaign.

Furthermore, we supplemented the dense light curves with the sparse-in-time photometric measurements from five different sky surveys. In particular, we used data from the Catalina Sky Survey (Larson et al. 2003), the US Naval Observatory in Flagstaff, ATLAS (Tonry et al. 2018a, 2018b; Heinze et al. 2018), the All-Sky Automated Survey for Supernovae (ASAS-SN; Shappee et al. 2014; Kochanek et al. 2017; Hanuš et al. 2021), and the Gaia Data Release 2 (Gaia Collaboration et al. 2018).

The optical data set for 203 allowed us to derive its unique spin state and 3D shape model solution. This object rotates with a sidereal rotation period of (24.05502 ± 0.00005) hr, and we provide two symmetric pole solutions following the standard ambiguity of the inversion method (Kaasalainen 2004). The appearance of the two shape models is shown in Figure A1.

[21] https://astro.troja.mff.cuni.cz/projects/damit/

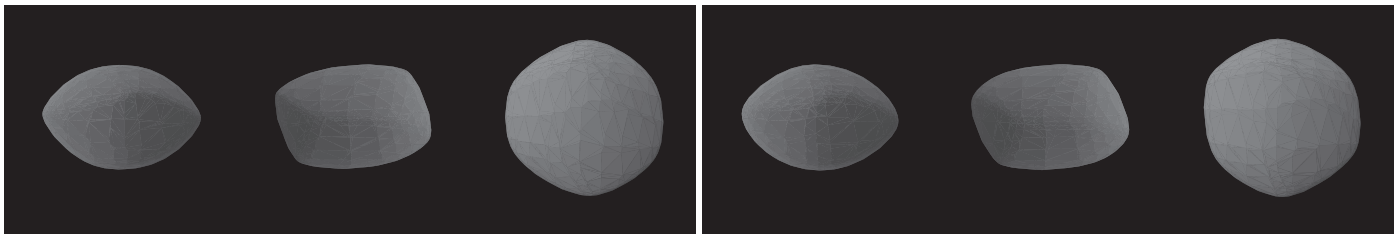

Figure A1. Convex shape models of 203 Pompeja. While the left panel represents the pole solution $\lambda_1 = 315$ [deg], $\beta_1 = -40$ [deg], the right panel shows the pole solution $\lambda_2 = 132$ [deg], $\beta_2 = -36$ [deg]. The left and middle views are equatorial with a 90° rotation, while the right view is pole-on. Both shape models appear very similar.

Appendix B
An NIR Observation of 203 Pompeja in 2021 January

The spectrum of 203 Pompeja measured on 2021 January 14 (Hasegawa et al. 2021) is much redder than the usual asteroids, which may cast doubt on the validity of the observations. One possibility could be that the spectrum was red due to slit misalignment. However, if the asteroid is out of alignment, the spectrum is blueing instead of reddening (Marsset et al. 2020). Therefore, in order for the asteroid to become red, it is the solar analog star observations that need to be misaligned. On the night we observed 203 (2021 January 14), we also observed five solar analog stars for the spectral division, four of which were spectrally very consistent (the fifth star was discarded). In addition, we observed NEAs 99942 Apophis and 2020 WU_5 on the same night as 203, and their respective spectra were consistent with previous and more recent observations (Figure B1). This provides strong credit to our 2021 observations of 203. Future spectroscopic observations and high angular resolution imaging of 203 acquired under high subobserver latitudes will help confirm or dismiss the existence of a fresh polar crater with a VRO spectrum on 203.

Appendix C
Visible Observations of Three Asteroids after 2020

Spectroscopic and spectrophotometric observations of three main belt asteroids, 212 Medea, 328 Gudrun, and 769 Tatjana, were performed with the Shelyak PF0021VIS–LISA spectrometer and the SBIG STX-16803 camera equipped with V-, R_C-, and I_C-band filters on the 1.0 m telescope at Seoul National University Astronomical Observatory (SAO), Seoul, Republic of Korea (Im et al. 2021), in 2020 or later. The procedures for the visible observations and reduction are as described in Hasegawa et al. (2021).

The spectroscopic data of this study yield classification of 212 Medea, 328 Gudrun, and 769 Tatjana as X, Cgh, and Xc types, respectively. The acquired spectra match previously obtained spectra (Figure C1). Therefore, it appears that the visible spectrum and spectrophotometric color reported in Hasegawa et al. (2021) are valid.

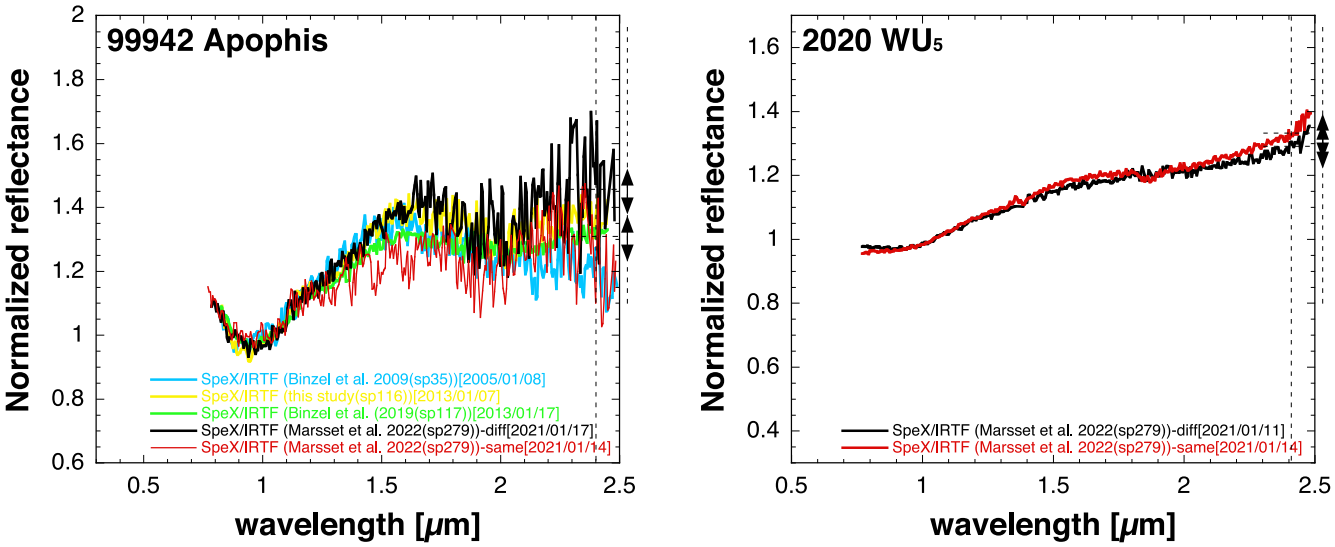

Figure B1. Spectra of 99942 Apophis (left panel) and 2020 WU_5 (right panel). The data of 203 Pompeja, 99942 Apophis, and 2020 WU_5 were taken on 2021 January 14. The spectra of 99942 and 2020 WU_5 were measured four times and once, respectively (Binzel et al. 2009, 2019; Marsset et al. 2022), in addition to their measurement on the same day as 203 (Hasegawa et al. 2021). The five spectra of 99942 and the two spectra of 2020 WU_5 are found to be in agreement. Square brackets in these panels indicate the observation dates. The black arrows indicate the slope uncertainty from Marsset et al. (2020) centered at the reflectance value of the spectra at 2.40 μm, as shown by the black dashed lines.

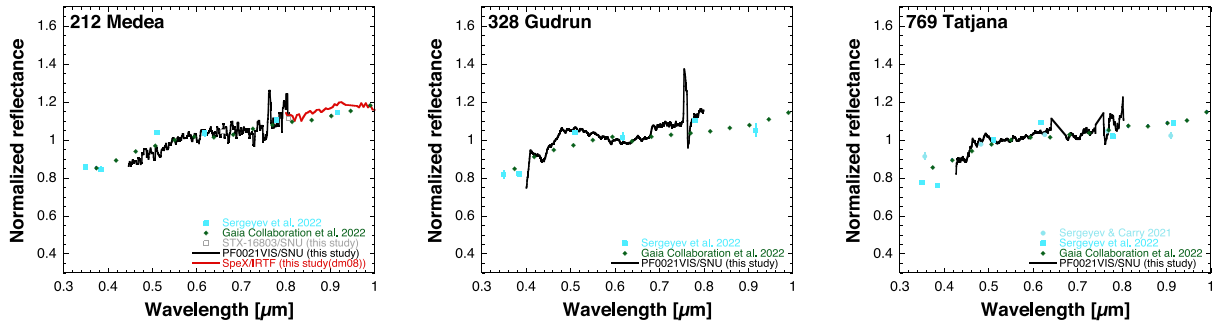

Figure C1. Spectra of 212 Medea, 328 Gudrun, and 769 Tatjana. The spectra of these asteroids were obtained at SAO in 2020–2021. Previous spectra were derived from Sergeyev & Carry (2021), Sergeyev et al. (2022), and Gaia Collaboration et al. (2022).

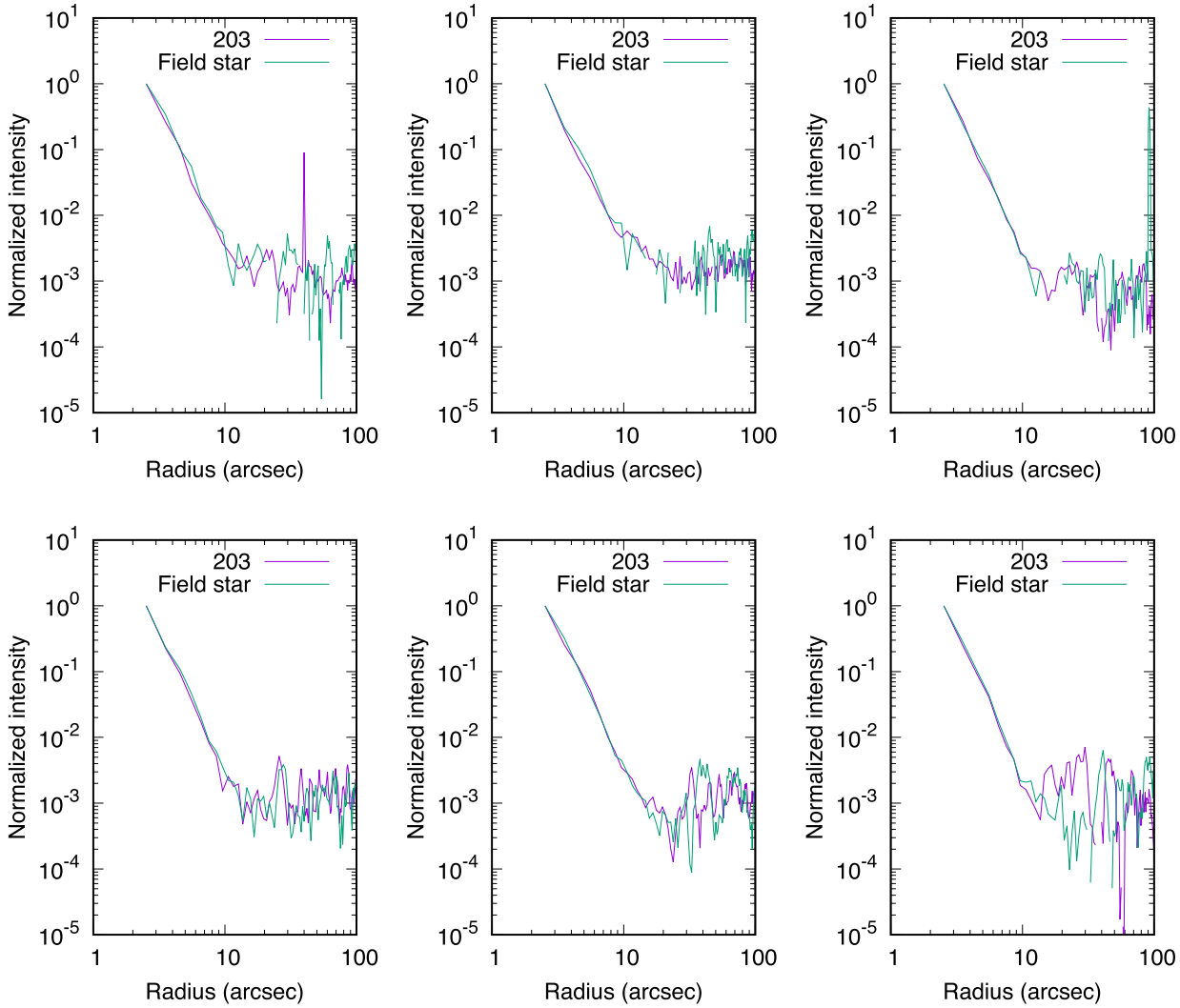

Figure D1. Radial brightness profiles of 203 Pompeja obtained by the Zwicky Transient Facility on 2020 December 10 (top left), 17 (top middle), and 22 (top right) and 2021 January 5 (bottom left), 13 (bottom middle), and 19 (bottom right). These profiles are normalized at 2.″5 from the photocenter and compared with field stars. The FWHM of the images used was roughly 2″–3″. Since 203 was almost saturated, brightness profiles within 2.″5 from the photocenter are not given.

Appendix D
Search for a Coma of 203 Pompeja

To confirm the comet-like activity of 203 Pompeja, radial brightness profiles of 203 and field stars around the observation date of Hasegawa et al. (2021) were examined. For comparison, images in the *r* band acquired at the 48 inch (1.2 m) Samuel Oschin Schmidt telescope in the Zwicky Transient Facility (Masci et al. 2019) were utilized.[22] The radial brightness profiles of 203 and field stars are consistent over a range of about 3 orders of magnitude, and no comet-like coma was detected around the observation date of Hasegawa et al. (2021; Figure D1).

[22] https://www.ipac.caltech.edu/doi/irsa/10.26131/IRSA539

ORCID iDs

Sunao Hasegawa https://orcid.org/0000-0001-6366-2608
Francesca E. DeMeo https://orcid.org/0000-0002-8397-4219
Michaël Marsset https://orcid.org/0000-0001-8617-2425
Josef Hanuš https://orcid.org/0000-0002-2934-3723
Chrysa Avdellidou https://orcid.org/0000-0001-8228-8789
Marco Delbo https://orcid.org/0000-0002-8963-2404
Schelte J. Bus https://orcid.org/0000-0003-4191-6536
Hidekazu Hanayama https://orcid.org/0000-0001-8221-6048
Takashi Horiuchi https://orcid.org/0000-0001-5925-3350
Driss Takir https://orcid.org/0000-0003-4942-2741
Emmanuël Jehin https://orcid.org/0000-0001-8923-488X
Marin Ferrais https://orcid.org/0000-0002-0535-652X
Jooyeon Geem https://orcid.org/0000-0002-3291-4056
Myungshin Im https://orcid.org/0000-0002-8537-6714
Yoonsoo P. Bach https://orcid.org/0000-0002-2618-1124
Sunho Jin https://orcid.org/0000-0002-0460-7550
Masateru Ishiguro https://orcid.org/0000-0002-7332-2479
Daisuke Kuroda https://orcid.org/0000-0002-7363-187X
Richard P. Binzel https://orcid.org/0000-0002-9995-7341
Akiko M. Nakamura https://orcid.org/0000-0001-6990-8496
Bin Yang https://orcid.org/0000-0002-5033-9593
Pierre Vernazza https://orcid.org/0000-0002-2564-6743

References

Athanasopoulos, D., Hanuš, J., Avdellidou, C., et al. 2022, A&A, in press
Avdellidou, C., Pajola, M., Lucchetti, A., et al. 2021, A&A, 656, L18
Bell, J. F., Izenberg, N. I., Lucey, P. G., et al. 2002, Icar, 155, 119
Betzler, A. S., Novaes, A. B., Santos, A. C. P., et al. 2012, MPBu, 39, 5
Binzel, R. P., Bus, S. J., Burbine, T. H., & Sunshine, J. M. 1996, Sci, 273, 946
Binzel, R. P., DeMeo, F. E., Burt, B. J., et al. 2015, Icar, 256, 22
Binzel, R. P., DeMeo, F. E., Turtelboom, E. V., et al. 2019, Icar, 324, 41
Binzel, R. P., Rivkin, A. S., Thomas, C. A., et al. 2009, Icar, 200, 480
Bourdelle de Micas, J., Fornasier, S., Delbo, M., et al. 2022, A&A, in press
Bus, S. J., & Binzel, R. P. 2002, Icar, 158, 106
Cellino, A., Bendjoya, P., Delbo', M., et al. 2020, A&A, 642, A80
Clark, B. E., Hapke, B., Pieters, C., & Britt, D. 2002, in Asteroid Space Weathering and Regolith Evolution, Asteroids III, ed. W. F. Bottke et al. (Tucson, AZ: Univ. Arizona Press), 585
DeMeo, F. E., Binzel, R. P., Slivan, S. M., & Bus, S. J. 2009, Icar, 202, 160
Di Martino, M. 1984, Icar, 60, 541
Dukes, C. A., Baragiola, R. A., & McFadden, L. A. 1999, JGR, 104, 1865
Durech, J., Sidorin, V., & Kaasalainen, M. 2010, A&A, 513, A46
Emery, J. P., Burr, D. M., & Cruikshank, D. P. 2011, AJ, 141, 25
Fatka, P., Moskovitz, N. A., Pravec, P., et al. 2022, MNRAS, 510, 6033
Fraser, W. C., Pike, R. E., Marsset, et al. 2022, PSJ, submitted, arXiv:2206.04068
Fulchignoni, M., Belskaya, I., Barucci, M. A., de Sanctis, M. C., & Doressoundiram, A. 2008, in Transneptunian Object Taxonomy, The solar system Beyond Neptune, ed. M. A. Barucci et al. (Tucson, AZ: Univ. Arizona Press), 181
Gaia Collaboration, Galluccio, L., Delbo, M., et al. 2022, A&A, in press
Gaia Collaboration, Spoto, F., Tanga, P., et al. 2018, A&A, 616, A13
Gold, T. 1955, MNRAS, 115, 585
Hanuš, J., Pejcha, O., Shappee, B. J., et al. 2021, A&A, 654, A48
Hapke, B., Cassidy, W., & Wells, E. 1975, Moon, 13, 339
Hasegawa, S., Marsset, M., DeMeo, F. E., et al. 2021, ApJL, 916, L6
Hasegawa, S., Marsset, M., DeMeo, F. E., et al. 2022, ApJL, 924, L9
Heinze, A. N., Tonry, J. L., Denneau, L., et al. 2018, AJ, 156, 241
Hiroi, T., Abe, M., Kitazato, K., et al. 2006, Natur, 443, 56
Hiroi, T., & Hasegawa, S. 2003, AMR, 16, 176
Hsieh, H. H., Yang, B., & Haghighipour, N. 2012, ApJ, 744, 9
Im, M., Kim, Y., Lee, C.-U., et al. 2021, JKAS, 54, 89
Ishiguro, M., Hanayama, H., Hasegawa, S., et al. 2011a, ApJL, 740, L11
Ishiguro, M., Hanayama, H., Hasegawa, S., et al. 2011b, ApJL, 741, L24
Jehin, E., Gillon, M., Queloz, D., et al. 2011, Msngr, 145, 2
Jewitt, D. 2012, AJ, 143, 66
Jin, S., & Ishiguro, M. 2022, A&A, in press
Kaasalainen, M. 2004, A&A, 422, L39
Kaasalainen, M., & Torppa, J. 2001, Icar, 153, 24
Kaasalainen, M., Torppa, J., & Muinonen, K. 2001, Icar, 153, 37
Keller, L. P., & McKay, D. S. 1993, Sci, 261, 1305
Kochanek, C. S., Shappee, B. J., Stanek, K. Z., et al. 2017, PASP, 129, 104502
Lantz, C., Binzel, R. P., & DeMeo, F. E. 2018, Icar, 302, 10
Lantz, C., Brunetto, R., Barucci, M. A., et al. 2017, Icar, 285, 43
Larson, S., Beshore, E., Hill, R., et al. 2003, BAAS, 35, 982
Lazzaro, D., Angeli, C., Carvano, J., et al. 2004, Icar, 172, 179
Marsset, M., DeMeo, F. E., Binzel, R. P., et al. 2020, ApJS, 247, 73
Marsset, M., DeMeo, F. E., Burt, B., et al. 2022, AJ, 163, 165
Masci, F. J., Laher, R. R., Rusholme, B., et al. 2019, PASP, 131, 018003
Masiero, J. R., Mainzer, A. K., Grav, T., et al. 2011, ApJ, 741, 68
Matsuoka, M., Nakamura, T., Kimura, Y., et al. 2015, Icar, 254, 135
Mommert, M. 2017, A&C, 18, 47
Moroz, L. V., Fisenko, A. V., Semjonova, L. F., Pieters, C. M., & Korotaeva, N. N. 1996, Icar, 122, 366
Nakamura, T., Noguchi, T., Tanaka, M., et al. 2011, Sci, 333, 1113
Nesvorný, D., Jedicke, R., Whiteley, R. J., & Ivezić, Ž. 2005, Icar, 173, 132
Noguchi, T., Kimura, M., Hashimoto, T., et al. 2014, M&PS, 49, 188
Noguchi, T., Nakamura, T., Kimura, M., et al. 2011, Sci, 333, 1121
Pieters, C. M., & McFadden, L. A. 1994, AREPS, 22, 457
Pilcher, F., Ferrero, A., Hamanowa, H., & Hamanowa, H. 2012, MPBu, 39, 99
Rayner, J. T., Toomey, D. W., Onaka, P. M., et al. 2003, PASP, 115, 362
Rivkin, A. S., Emery, J. P., Howell, E. S., et al. 2022, PSJ, 3, 153
Sanchez, J. A., Reddy, V., Nathues, A., et al. 2012, Icar, 220, 36
Sawyer, S. R. 1991, PhD thesis, Univ. of Texas, Austin
Sergeyev, A. V., & Carry, B. 2021, A&A, 652, A59
Sergeyev, A. V., Carry, B., Onken, C. A., et al. 2022, A&A, 658, A109
Shappee, B. J., Prieto, J. L., Grupe, D., et al. 2014, ApJ, 788, 48
Shevchenko, V. G., Belskaya, I. N., Muinonen, K., et al. 2016, P&SS, 123, 101
Takir, D., & Emery, J. P. 2012, Icar, 219, 641
Tedesco, E. F., Noah, P. V., Noah, M., & Price, S. D. 2002, AJ, 123, 1056
Thomas, C. A., Emery, J. P., Trilling, D. E., et al. 2014, Icar, 228, 217
Tody, D. 1993, in ASP Conf. Ser., 52, Astronomical Data Analysis Software and Systems II, ed. R. J. Hanisch, R. J. V. Brissenden, & J. Barnes (San Francisco, CA: ASP), 173
Tonry, J. L., Denneau, L., Flewelling, H., et al. 2018b, ApJ, 867, 105
Tonry, J. L., Denneau, L., Heinze, A. N., et al. 2018a, PASP, 130, 064505
Trigo-Rodriguez, J. M., García-Hernández, D. A., Montañés-Rodríguez, P., et al. 2011, in EPSC-DPS Joint Meeting 2011, 264
Usui, F., Kuroda, D., Müller, T. G., et al. 2011, PASJ, 63, 1117
Vernazza, P., Binzel, R. P., Rossi, A., Fulchignoni, M., & Birlan, M. 2009, Natur, 458, 993
Vernazza, P., Ferrais, M., Jorda, L., et al. 2021, A&A, 654, A56
Vernazza, P., Fulvio, D., Brunetto, R., et al. 2013, Icar, 225, 517
Veverka, J., Robinson, M., Thomas, P., et al. 2000, Sci, 289, 2088
Veverka, J., Thomas, P., Harch, A., et al. 1997, Sci, 278, 2109
Xu, S., Binzel, R. P., Burbine, T. H., & Bus, S. J. 1995, Icar, 115, 1
Yamada, M., Sasaki, S., Nagahara, H., et al. 1999, EP&S, 51, 1265
Yanagisawa, K., Kuroda, D., Yoshida, M., et al. 2010, in AIP Conf. Ser., 1279, Deciphering the Ancient Universe with Gamma-ray Bursts, ed. N. Kawai & S. Nagataki (Melville, NY: AIP), 466
Yang, B., & Hsieh, H. 2011, ApJL, 737, L39
Yurimoto, H., Abe, K.-i., Abe, M., et al. 2011, Sci, 333, 1116